

Design and Development of a Medical Parallel Robot for Cardiopulmonary Resuscitation

Yangmin Li, *Senior Member, IEEE*, and Qingsong Xu

Abstract—The concept of a medical parallel robot applicable to chest compression in the process of cardiopulmonary resuscitation (CPR) is proposed in this paper. According to the requirement of CPR action, a three-prismatic-universal-universal (3-PUU) translational parallel manipulator (TPM) is designed and developed for such applications, and a detailed analysis has been performed for the 3-PUU TPM involving the issues of kinematics, dynamics, and control. In view of the physical constraints imposed by mechanical joints, both the robot-reachable workspace and the maximum inscribed cylinder-usable workspace are determined. Moreover, the singularity analysis is carried out via the screw theory, and the robot architecture is optimized to obtain a large well-conditioning usable workspace. Based on the principle of virtual work with a simplifying hypothesis adopted, the dynamic model is established, and dynamic control utilizing computed torque method is implemented. At last, the experimental results made for the prototype illustrate the performance of the control algorithm well. This research will lay a good foundation for the development of a medical robot to assist in CPR operation.

Index Terms—Control, design theory, dynamics, medical robots, parallel manipulators.

I. INTRODUCTION

IN the case of a patient being in cardiac arrest, cardiopulmonary resuscitation (CPR) must be applied in both rescue breathing (mouth-to-mouth resuscitation) and chest compressions. Generally, the compression frequency for an adult is at the rate of about 100 times per minute with the depth of 4–5 cm using two hands, and the CPR is usually performed with the compression-to-ventilation ratio of 15 compressions to two breaths,¹ so as to maintain oxygenated blood flowing to vital organs and to prevent anoxic tissue damage during cardiac arrest [1]. Without oxygen, permanent brain damage or death can occur in less than 10 min. Thus, for a large number of patients who undergo unexpected cardiac arrest, the only hope of survival is timely application of CPR.

However, some patients in cardiac arrest may also be infected with other indeterminate diseases, and hence, it is very dangerous for a doctor to apply CPR directly to them. For example, before the severe acute respiratory syndrome (SARS) was first recognized as a global threat in 2003, in many hospitals, such kinds of patients were rescued as usual, and some doctors who

had performed CPR on such patients were unfortunately infected with the SARS corona virus [2]. In addition, chest compressions consume a lot of energy from doctors; for instance, sometimes it is necessary for ten doctors to work for 2 h to perform chest compressions to rescue a patient in a Beijing, China, hospital. Therefore, a medical robot that can be used for chest compressions is urgently required. In view of this practical requirement, we will design and develop a medical parallel robot to assist in CPR operation and desire that the robot can perform this job well instead of doctors.

A parallel manipulator generally consists of a moving platform that is connected to a fixed base by several limbs or legs in parallel. Nowadays, parallel manipulators are applied widely since they possess many inherent advantages in terms of high speed, high accuracy, high stiffness, and high load-carrying capacity over their serial counterparts. The enumeration of parallel robots' mechanical architectures and their versatile applications can be found in [3] and [4], and some new architectures have been proposed more recently in the literature [5]–[9].

In particular, parallel manipulators have great potential applications in medical fields, thanks to their fine characteristics of stiffness, positioning accuracy, etc. For example, a new approach to robot-assisted spine and trauma surgery was presented in [10] utilizing a designed 6-DOF parallel manipulator. Training for opening and closing of the mouth for the rehabilitation of patients with problems of the jaw joint was suggested in [11] using a 6-DOF parallel robot, and a 4-DOF parallel wire-driven mechanism was presented in [12] with applications to leg rehabilitation, etc. However, to the authors' knowledge, nothing in the literature can be found that deals with parallel robots that can be applied in CPR assistance up to now.

The remainder of this paper is organized as follows. The conceptual design of the medical robot system is proposed in Section II. The kinematics analysis is carried out in Section III, where the reachable workspace of the manipulator is generated, and all the singularities are identified. Section IV is focused on the optimal design of the robot architecture using a mixed performance index. The dynamic modeling and dynamic control method are presented in Section V. Then, in Section VI, the hardware development for the medical robot is accomplished, and the experimental studies with a model-based control algorithm are undertaken. Finally, this paper concludes with a discussion of future research considerations in Section VII.

II. CONCEPTUAL DESIGN OF A CPR ROBOT SYSTEM

A schematic of performing CPR is shown in Fig. 1, and a conceptual design of the medical robot system is illustrated in

Manuscript received March 1, 2006; revised December 15, 2006. Recommended by Guest Editors H.-P. Huang and F.-T. Cheng. This work was supported in part by the research committee of the University of Macau under Grant RG068/05-06S/LYM/FST and in part by the Macao Science and Technology Development Fund under Grant 069/2005/A.

The authors are with the Department of Electromechanical Engineering, Faculty of Science and Technology, University of Macau, Macao SAR, China (e-mail: ymli@umac.mo; ya47401@umac.mo).

Digital Object Identifier 10.1109/TMECH.2007.897257

¹<http://www.health.harvard.edu/fhg/firstaid/CPRadult.shtml>, 2003

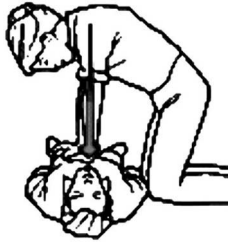


Fig. 1. Schematic of CPR operation.

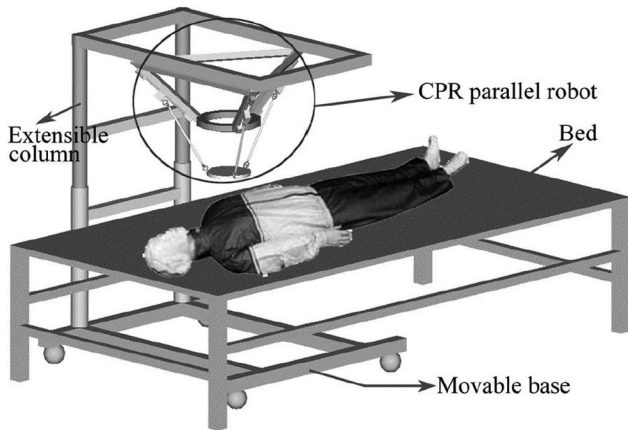


Fig. 2. Conceptual design of a CPR medical robot system.

Fig. 2. As shown in Fig. 2, the patient is placed on a bed beside a CPR robot, which is mounted on a separated movable base via two supporting columns and is deposited above the chest of the patient. The movable base can be moved anywhere on the ground, and the supporting columns are extensible in the vertical direction. Thus, the robot can be positioned well by hand such that the chest compressions may start as soon as possible, which also allows a doctor to easily take the robot away from the patient in the case of any erroneous operation. Moreover, the CPR robot is located on one side of the patient, thereby providing a free space for a rescuer to access the patient on the other side.

In view of the high-stiffness and high-accuracy properties, parallel mechanisms are employed to design such a manipulator applicable to chest compressions in CPR. This idea is motivated from the reason why the rescuer uses two hands instead of only one hand to perform the action of chest compressions. In the process of performing chest compressions, the two arms of the rescuer construct a parallel mechanism. The main disadvantage of parallel robots is their relatively limited workspace range. Fortunately, by a proper design, a parallel robot is able to satisfy the workspace requirement with a height of 4–5 cm for the CPR operation.

In the next step comes the problem of how to select a particular parallel robot for the application of CPR, since, nowadays, there exist many parallel robots providing various types of output motions. An observation of the chest compressions in manual CPR reveals that the most useful motion adopted in such an application is the back-and-forth translation in a direction vertical to the patient's chest, whereas the rotational motions are almost

useless. Thus, parallel robots with a total of 6 DOF are not necessarily required here. In addition, a 6-DOF parallel robot usually possesses some disadvantages in terms of complicated forward kinematics problems and highly coupled translation and rotation motions, etc., which complicate the control of such robots. Hence, translational parallel manipulators (TPMs) with only three translational DOF in space are sufficient to be employed in CPR operation. Because in addition to a translation, vertical to the chest of the patient, a 3-DOF TPM can also provide translations in any other direction, this enables the adjustment of the manipulator's moving platform to a suitable position to perform chest compression tasks. At this point, TPMs with less than 3 DOF are not adopted here.

As far as a 3-DOF TPM is concerned, it can be designed as various architectures with different mechanical joints. Many TPMs can be found in the literature [13]–[19]. In some types of these TPMs, the first joint of each limb is located at the base. In this case, since the actuators can be mounted on the base, the moving components of the manipulator do not bear any load of the actuators. This enables large powerful actuators to drive relatively small structures, facilitating the design of the manipulator with faster, stiffer, and stronger characteristics. Several existing TPMs fall into this category, such as the Delta and linear-Delta-architecture-like TPMs [13]–[15], three-prismatic-universal-universal (3-PUU) and three-revolute-universal-universal (3-RUU) mechanisms [16], etc.

From the economic point of view, the simpler the architecture of a TPM, the lower will be the cost. In view of the complexity of the TPM topology, including the number of mechanical joints and links and their manufacture procedures, a 3-PUU TPM is finally chosen and built utilizing the hardware available at the Mechatronics Laboratory, University of Macau. It should be noted that, theoretically, other architectures such as the Delta or linear-Delta-like TPMs can also be employed in a CPR robot system.

For the purposes of design and development of a 3-PUU medical parallel robot for CPR applications, it is necessary to investigate the fundamental issues of the robot in terms of kinematic modeling and optimization, workspace determination, dynamic modeling, and so on, which will be performed in detail in the following sections.

III. KINEMATIC ANALYSIS OF THE MEDICAL ROBOT

A. Architecture Description

As shown in Figs. 2 and 3, the 3-PUU TPM consists of a moving platform, a fixed base, and three limbs with identical kinematic structure. Each limb connects the fixed base to the moving platform by a prismatic (P) joint followed by two universal (U) joints in sequence, where the P joint is driven by a linear actuator. In view of the cost effectiveness, the linear actuator is implemented by using a lead screw actuation system driven by a dc servomotor in this paper. For safety reasons, the selected screw should satisfy the condition of self-locking, i.e., the lead angle of the lead screw is less than the angle of friction, so as to ensure that the nut is self-locking when the lead screw is

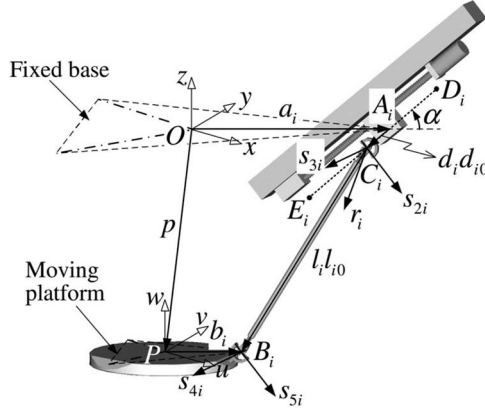


Fig. 3. Representation of vectors and joint axes for the i th limb.

not actuated. It should be noted that if other types of linear actuators are selected, they should not be back-drivable for safety reasons as well.

Similar to a 3-UPU platform [18], [19], it can be demonstrated that a 3-PUU mechanism can be arranged to achieve 3-DOF translational motion with certain geometric conditions satisfied. Briefly, in each kinematic chain, the first revolute joint axis is parallel to the last revolute joint axis, and the two intermediate joint axes are parallel to each other, i.e., the unit vectors of joint axes $\mathbf{s}_{3i} = \mathbf{s}_{4i}$ and $\mathbf{s}_{2i} = \mathbf{s}_{5i}$ ($i = 1, 2$, and 3), as shown in Fig. 3.

For the sake of analysis, we assign a fixed Cartesian reference frame $O\{x, y, z\}$ at the center point O of the fixed base platform $\Delta A_1 A_2 A_3$, and a moving frame $P\{u, v, w\}$ on the moving platform at the center point P of triangle $\Delta B_1 B_2 B_3$. In addition, let the x - and u -axes be parallel to each other, and the x -axis be direct along $\overrightarrow{OA_1}$. The angle between vectors $\overrightarrow{OA_i}$ and $\overrightarrow{PB_i}$ is defined as the twist angle θ , i.e., the angle between the moving and base platforms. In addition, the three rails $D_i E_i$ intersect the $x - y$ plane at points A_1, A_2 , and A_3 that lie on a circle of radius a . The three links $C_i B_i$ with the length of l intersect the $u - v$ plane at points B_1, B_2 , and B_3 , which lie on a circle of radius b . Angle α is measured from the fixed base to rails $D_i E_i$ and is defined as the layout angle of actuators. In order to achieve a symmetric workspace of the manipulator, both $\Delta A_1 A_2 A_3$ and $\Delta B_1 B_2 B_3$ are assigned to be equilateral triangles.

Additionally, the joint axis orientations of \mathbf{s}_{2i} and \mathbf{s}_{5i} are assembled to be perpendicular to the rail direction $\overrightarrow{D_i E_i}$ and lie in a plane defined by vectors $\overrightarrow{OA_i}$ and $\overrightarrow{D_i E_i}$. Joint axes \mathbf{s}_{3i} and \mathbf{s}_{4i} are all perpendicular to the leg direction of $\overrightarrow{C_i B_i}$.

B. Kinematic Modeling

Let \mathbf{l}_{i0} be a unit vector along the leg $C_i B_i$, d_i represents a linear displacement of the i th actuator, and \mathbf{d}_{i0} denotes the corresponding unit vector pointing along rail $D_i E_i$. Also, let $\mathbf{a}_i = \overrightarrow{OA_i}$, $\mathbf{b}_i = \overrightarrow{PB_i}$, and $\mathbf{p} = \overrightarrow{OP} = [x \ y \ z]^T$. With reference to Fig. 3, a vector-loop equation can be written for the i th limb

$$l \mathbf{l}_{i0} = \mathbf{l}_i - d_i \mathbf{d}_{i0} \quad (1)$$

where $\mathbf{l}_i = \mathbf{p} + \mathbf{b}_i - \mathbf{a}_i$.

Considering a lead screw actuation system, the rotation θ_i of the lead screw can be converted to the linear displacement d_i of the nut as

$$d_i = p \theta_i / (2\pi) \quad (2)$$

where p denotes the thread lead of the lead screw.

The inverse kinematics problem calculates the actuated variables from a given position of the moving platform, which can be easily solved in the closed form with the consideration of (1) and (2). On the other hand, given a set of actuated inputs, the moving platform position is solved by the forward kinematics. Similar to most of the 3-DOF TPMs [14], the forward kinematics of a 3-PUU TPM can be solved by determining the intersection of three spheres, and more details can be found in [20].

Differentiating (1) with respect to time and eliminating passive variables, one can generate [21]

$$\mathbf{J}_q \dot{\mathbf{q}} = \mathbf{J}_x \dot{\mathbf{x}} \quad (3)$$

where

$$\mathbf{J}_q = \begin{bmatrix} \mathbf{1}_{10}^T \mathbf{d}_{10} & 0 & 0 \\ 0 & \mathbf{1}_{20}^T \mathbf{d}_{20} & 0 \\ 0 & 0 & \mathbf{1}_{30}^T \mathbf{d}_{30} \end{bmatrix}, \quad \mathbf{J}_x = \begin{bmatrix} \mathbf{1}_{10}^T \\ \mathbf{1}_{20}^T \\ \mathbf{1}_{30}^T \end{bmatrix} \quad (4)$$

and $\dot{\mathbf{q}} = [\dot{d}_1 \ \dot{d}_2 \ \dot{d}_3]^T$ is the vector of linear actuated joint rates. When the manipulator is away from singularities, from (3), we can obtain that

$$\dot{\mathbf{q}} = \mathbf{J} \dot{\mathbf{x}} \quad (5)$$

where $\mathbf{J} = \mathbf{J}_q^{-1} \mathbf{J}_x$ is the 3×3 Jacobian matrix of a 3-PUU TPM, which relates the output velocities to the actuated joint rates.

C. Workspace Determination

In the design of a 3-PUU TPM, the physical constraints in terms of motion limits of mechanical joints, interference between links and the surrounding, self-collision, etc., should be taken into account. For the sake of brevity, we only consider the translational limits of the actuated P joints and rotational limits of the passive U joints and assume that the interference and collision problems can be avoided by restricting the motion limits of the mechanical joints.

Let the translational limits of actuated P joints be $\pm S$, i.e., $-S \leq d_i \leq S$ ($i = 1, 2, 3$), and the rotational limits of passive U joints be $\pm \varphi$, which forms a pyramid-shaped range for each leg. In view of the fact that the moving platform is parallel to the base platform, it is clear that the constraint motion of point P induced by the i th limb can be derived from the possible motion of point B_i by a constant translation of vector $\overrightarrow{B_i P}$. Hence, the TPM workspace can be determined as the intersection of the possible motion range of B_i , i.e., the workspace of each leg [20].

Assume that $S = 50$ mm and $\varphi = 22^\circ$, the reachable workspace of a 3-PUU TPM with the architectural parameters described in Table I is sketched in Fig. 4, which is generated by utilizing a geometric approach. It can be noticed that the cross section of the workspace can also be calculated exactly by using Green's theorem [22].

TABLE I
ARCHITECTURAL PARAMETERS OF A 3-PUU TPM

Parameter	Value	Unit	Parameter	Value	Unit
a	150.0	mm	α	45.0	$^\circ$
b	20.0	mm	θ	0.0	$^\circ$
l	180.0	mm	φ	22.0	$^\circ$
S	50.0	mm			

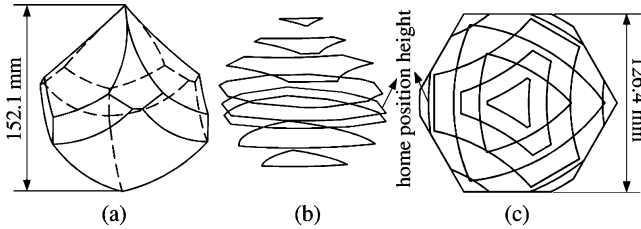


Fig. 4. Reachable workspace of a 3-PUU TPM. (a) 3-D view. (b) Cross sections at different heights. (c) Top view.

It can be observed that the workspace is 120° symmetrical about the three linear actuators' motion directions from up to down view. In the upper and lower ranges of the workspace, the cross section has the triangular shape, while in the dominated middle range, the cross-sectional shape looks like a hexagon.

D. Singularity Identification

The identification of singularities is important both for singularity-free path planning and control implementation thereafter. Usually, the singularity analysis of a parallel robot can be successfully performed based on the rank deficiency of the Jacobian matrix [21]. However, similar to a 3-UPU platform [23], [24], the 3×3 Jacobian (\mathbf{J}) for a 3-PUU TPM is not sufficient to predict all the singularities including the architecture singularity [23] and constraint singularity [25]. In contrast, the singular configurations can be fully identified by resorting to the screw theory as reported in [26].

With \mathbf{v} and $\boldsymbol{\omega}$ respectively denoting the vectors for the linear and angular velocities, the twist of the moving platform can be defined as $\mathbf{T} = [\mathbf{v}^T \ \boldsymbol{\omega}^T]^T$ in Plücker axis coordinate. Concerning a 3-PUU TPM, the connectivity of each limb is equal to five, and hence, the instantaneous twist \mathbf{T} of the moving platform can be expressed as a linear combination of the five instantaneous twists, i.e.

$$\mathbf{T} = \dot{d}_1 \hat{\mathbf{T}}_{1i} + \dot{\theta}_{2i} \hat{\mathbf{T}}_{2i} + \dot{\theta}_{3i} \hat{\mathbf{T}}_{3i} + \dot{\theta}_{4i} \hat{\mathbf{T}}_{4i} + \dot{\theta}_{5i} \hat{\mathbf{T}}_{5i} \quad (6)$$

for $i = 1, 2$, and 3 , where $\dot{\theta}_{ji}$ is the intensity, and $\hat{\mathbf{T}}_{ji}$ denotes a unit screw associated with the j th joint of the i th limb, and

$$\hat{\mathbf{T}}_{1i} = \begin{bmatrix} \mathbf{d}_{i0} \\ \mathbf{0} \end{bmatrix}, \quad \hat{\mathbf{T}}_{2i} = \begin{bmatrix} \mathbf{c}_i \times \mathbf{s}_{2i} \\ \mathbf{s}_{2i} \end{bmatrix}, \quad \hat{\mathbf{T}}_{3i} = \begin{bmatrix} \mathbf{c}_i \times \mathbf{s}_{3i} \\ \mathbf{s}_{3i} \end{bmatrix},$$

$$\hat{\mathbf{T}}_{4i} = \begin{bmatrix} \mathbf{b}_i \times \mathbf{s}_{4i} \\ \mathbf{s}_{4i} \end{bmatrix}, \quad \hat{\mathbf{T}}_{5i} = \begin{bmatrix} \mathbf{b}_i \times \mathbf{s}_{5i} \\ \mathbf{s}_{5i} \end{bmatrix}$$

can be identified, where $\mathbf{0}$ denotes a 3×1 zero vector, \mathbf{s}_{ji} represents a unit vector along the j th joint axis of the i th limb, and $\mathbf{c}_i = \mathbf{b}_i - l\mathbf{l}_{i0}$.

Firstly, it follows that one screw $\hat{\mathbf{t}}_{ci}$ (expressed in Plücker ray coordinate) that is reciprocal to all the joint screws of the i th limb forms a one-system, and can be identified as an infinite pitch screw with a direction perpendicular to the two joint axes of a U joint, i.e.,

$$\hat{\mathbf{t}}_{ci} = \begin{bmatrix} \mathbf{0} \\ \mathbf{r}_i \end{bmatrix} \quad (7)$$

where \mathbf{r}_i is a unit vector along the direction defined by $\mathbf{s}_{2i} \times \mathbf{s}_{3i}$ (or $\mathbf{s}_{5i} \times \mathbf{s}_{4i}$), as shown in Fig. 3.

Taking the reciprocal product of both sides of (6) with $\hat{\mathbf{t}}_{ci}$ and rewriting the results into the matrix form, yields

$$\mathbf{J}_c \mathbf{T} = \mathbf{0} \quad (8)$$

where

$$\mathbf{J}_c = \begin{bmatrix} \mathbf{0} & \mathbf{r}_1^T \\ \mathbf{0} & \mathbf{r}_2^T \\ \mathbf{0} & \mathbf{r}_3^T \end{bmatrix}_{3 \times 6} \quad (9)$$

is called the Jacobian of constraints [26].

Each row in \mathbf{J}_c denotes a moment of constraints imposed by the joints of a limb, the combination of which constrains the moving platform a 3-DOF motion. Hence, if the three moments with directions of \mathbf{r}_i are linearly independent, the unique solution to (8) is $\boldsymbol{\omega} = \mathbf{0}$, which means the absence of the rotational DOF. However, if the three moments lie on a common plane or are parallel to one another, the TPM will be under constraint singularity, where the TPM gets additional rotational DOF. The existence of constraint singularity can be verified by checking whether the determinant of \mathbf{J}_c vanishes or not.

Secondly, with the actuators locked, the reciprocal screws of each limb form a two-system which includes the screw $\hat{\mathbf{t}}_{ci}$ identified earlier. One additional basis screw $\hat{\mathbf{t}}_{ai}$ being reciprocal to all the passive joint screws of the i th limb can be identified as a zero pitch screw along the direction passing through the centers of the two U joints

$$\hat{\mathbf{t}}_{ai} = \begin{bmatrix} \mathbf{l}_{i0} \\ \mathbf{b}_i \times \mathbf{l}_{i0} \end{bmatrix}. \quad (10)$$

Similarly, taking the reciprocal product on both sides of (6) with $\hat{\mathbf{t}}_{ai}$, results in

$$\mathbf{J}_a \mathbf{T} = \mathbf{J}_q \dot{\mathbf{q}} \quad (11)$$

where \mathbf{J}_q is the inverse Jacobian, as expressed in (4), $\dot{\mathbf{q}} = [\dot{d}_1 \ \dot{d}_2 \ \dot{d}_3]^T$ denotes the actuated joint rates, and

$$\mathbf{J}_a = \begin{bmatrix} \mathbf{l}_{10}^T & (\mathbf{b}_1 \times \mathbf{l}_{10})^T \\ \mathbf{l}_{20}^T & (\mathbf{b}_2 \times \mathbf{l}_{20})^T \\ \mathbf{l}_{30}^T & (\mathbf{b}_3 \times \mathbf{l}_{30})^T \end{bmatrix}_{3 \times 6} \quad (12)$$

is defined as the Jacobian of actuation.

Each row in \mathbf{J}_a denotes a force of actuation contributing along a leg. Once the three forces with directions of \mathbf{l}_{i0} are linearly dependent, the TPM will be under architecture singularity. It is the case when the three legs lie on a common plane or are parallel to each other. Under this type of singularity, with the

actuators locked, the moving platform of the TPM can still undergo infinitesimal translations.

In addition, the inverse singularity will occur in case if the Jacobian \mathbf{J}_q is not of full rank. From (4), one can see that this is the case of $\mathbf{l}_{i0}^T \mathbf{d}_{i0} = 0$ for $i = 1, 2$, or 3 , i.e., the directions of one or more of legs are perpendicular to the axial directions of the corresponding actuated joints. In such situations, the moving platform loses one or more DOF.

Furthermore, associating (8) with (11) allows the generation of

$$\dot{\mathbf{q}}_o = \mathbf{J}_o \mathbf{T} \quad (13)$$

where $\dot{\mathbf{q}}_o = [\dot{d}_1 \ \dot{d}_2 \ \dot{d}_3 \ 0 \ 0 \ 0]^T$ is a vector of expanded joint rates, and

$$\mathbf{J}_o = \begin{bmatrix} \mathbf{J}_q^{-1} \mathbf{J}_a \\ \mathbf{J}_c \end{bmatrix} \quad (14)$$

is called the 6×6 overall Jacobian of a 3-PUU TPM, which can be employed to evaluate all the singularity properties of the TPM.

IV. ARCHITECTURE OPTIMIZATION FOR A LARGE SINGULARITY-FREE USABLE WORKSPACE

To design a parallel robot, there are many factors that have to be taken into account [27]–[29]. In order to design a medical robot, the safety of the patient is the first and foremost issue needed to be kept in mind. As far as the design criteria for a 3-PUU medical parallel robot are concerned, the most important issue is to design the medical robot without singularities within its workspace. Because the singularity results in the loss of controllability of the robot, under such situations, the patient will probably be harmed. Another issue that needs to be considered is the accuracy of the robot, which can be mainly solved by means of calibration. In this section, the architecture of the medical robot will be optimized to generate a large usable workspace excluding the singularities.

It is known that the conditioning index (CI) is defined as the reciprocal of the condition number of the Jacobian matrix [30], [31], that is,

$$\mu = \frac{1}{\kappa} \quad (15)$$

where κ denotes the condition number of the Jacobian matrix. However, a problem arises for the condition number as far as the units of elements in the Jacobian matrix are concerned. An observation of the Jacobian \mathbf{J}_o in (14) reveals that the first three columns are dimensionless while the last three columns have the unit of length. In order to homogenize the dimension of the overall Jacobian, the last three columns can be divided by the radius of the moving platform [32], thus, leading to a homogeneous overall Jacobian for a 3-PUU TPM

$$\mathbf{J}_{oh} = \begin{bmatrix} \mathbf{J}_{ah} \\ \mathbf{J}_c \end{bmatrix} \quad (16)$$

where $\mathbf{J}_{ah} = \mathbf{J}_q^{-1} \mathbf{J}_a \mathbf{d}$, with $\mathbf{d} = \text{diag}\{1 \ 1 \ 1 \ \frac{1}{b} \ \frac{1}{b} \ \frac{1}{b}\}$.

The CI is bounded between 0 (singularity) and 1 (isotropy), and measures the degree of ill-conditioning of the Jacobian

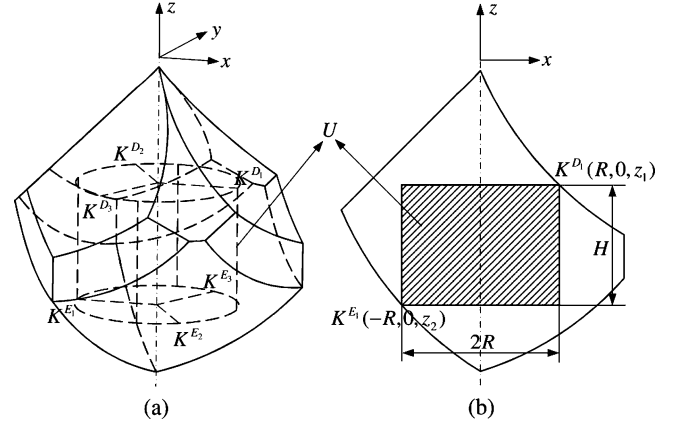


Fig. 5. Determination of cylinder-usable workspace U . (a) 3-D view. (b) x - z section view.

matrix, i.e., closeness of the singularity. Thus, CI can be used to evaluate the singularity of a manipulator. In the design of the medical robot, it is expected that singular configurations are far away from the manipulator workspace, which can be satisfied by ensuring that the CI values over the workspace are all larger than a specified value.

In addition, a global dexterity index (GDI) is given in [31]

$$\varepsilon = \frac{\int_V \mu dV}{V} \quad (17)$$

where V is the total workspace volume. The GDI describes the uniformity of manipulability over the entire workspace and can also be adopted to evaluate the conditioning of the Jacobian matrix.

A. Determination of the Maximum Usable Workspace

A visualization of CI distribution in the planes at different heights within the workspace reveals that the worst CI occurs around the boundary of the lowest plane. This comes from the reason that the manipulator approaches singularity when it is near the workspace boundary. Thus, it is reasonable to restrict the manipulator to perform tasks in a usable workspace, i.e., a subworkspace located within the reachable workspace. Concerning a 3-PUU TPM for the CPR medical application, we define the usable workspace as the maximum inscribed cylinder inside the reachable workspace with its central axis along the z -axis direction.

The determination procedure for such a cylinder usable workspace (U) with the radius R and height H is illustrated in Fig. 5. It is observed that the workspace U inscribed in the reachable workspace at six points of K^{D_i} and K^{E_i} ($i = 1, 2, 3$), which lie on the surfaces of the six spheres centered at D_i and E_i , respectively. The volume of U can be calculated by

$$V_U = \pi R^2 H = \pi R^2 (z_1 - z_2) \quad (18)$$

where $z_1 = Ss\alpha - [l^2 - (R - a - Sca + b)^2]^{1/2}$ and $z_2 = -Ss\alpha - [l^2 - (R + a - Sca - b)^2]^{1/2}$, with $s\alpha = \sin(\alpha)$ and $c\alpha = \cos(\alpha)$, respectively.

For any 3-PUU TPM, the maximum volume of the usable workspace arises in the case of $\frac{\partial V_U}{\partial R} = 0$, which represents an equation in a single variable R and allows the calculation of the values of R and H in sequence.

B. Design Variables and Objective Function

The architectural parameters of a 3-PUU TPM involve the sizes of base platform (a) and moving platform (b), length of legs (l), layout angle of actuators (α), and the twist angle (θ). To obtain a symmetric workspace, the twist angle is designed as $\theta = 0^\circ$, and in order to perform the architecture optimization independent of the dimension of each design candidate, the first three parameters are scaled by S , i.e., the half stroke of linear actuators. Thus, the design variables become $\frac{a}{S}$, $\frac{b}{S}$, $\frac{l}{S}$, and α . Additionally, to ensure a real geometry of the robot, the design variables are restricted within the parameter spaces of $[0.5 \ 5.0]$, $[0.5 \ 5.0]$, $[1.0 \ 5.0]$, and $[0^\circ \ 90^\circ]$, respectively.

Regarding the physical constraints, the rotational limits of U joints are $\varphi = 22^\circ$, the motion range limits of P joints are $\pm S$, and the home position of the moving platform is assigned as the middle stroke of linear actuators, i.e., $d_i = 0$ ($i = 1, 2, 3$).

The optimization objective for the 3-PUU medical parallel robot is to obtain a usable workspace with the best conditioning. The objective function for maximization is defined as the minimum value of a mixed index, which is a weighted sum of CI (μ) and GDI (ε) over the whole usable workspace (U)

$$f(n) = \min_{i \in U} \{w_c \mu_i + (1 - w_c) \varepsilon_i\} \quad (19)$$

where $n = [\frac{a}{S} \ \frac{b}{S} \ \frac{l}{S} \ \alpha]^T$ are the design variables, and the weight parameter w_c describes the proportion of CI in the mixed index.

C. Computational Issues and Optimization Results

In the optimal design to search a robot geometry with the maximum value of objective function $f(n)$, the search space, i.e., the parameter space, of each design variable is sampled at regular intervals. Each sampling node represents the geometry of a particular robot. The performance of the robot corresponding to each node is evaluated by the mixed index.

Considering the CI distributions within the reachable workspace, i.e., the minimal CI value occurs on the circular boundary of the usable workspace bottom, the overall performance is evaluated on the two end circular planes of the usable workspace by a discretization method. Each plane is sampled in terms of radius and angle in a polar coordinate, where one circle is sampled by the interval of 60° . This is reasonable since the distributions of CI inside the workspace have a symmetry at 120° just similar to the shape of workspace, and the radius (R) of the usable workspace is sampled as five line segments.

In addition, the design parameters of $\frac{a}{S}$, $\frac{b}{S}$, $\frac{l}{S}$, and α are sampled by the interval of 0.5, 0.5, 0.5, and 15° , respectively. The optimization is carried out on a personal computer (Intel Pentium 4 CPU 3.00-GHz, 512-MB RAM) with Microsoft Windows XP operating system. For the optimization with a particular weight number (w_c), the computational time is about 2.0 h, and the nu-

merical results for $w_c = 0.5$ are: $\frac{a}{S} = 4.5$, $\frac{b}{S} = 0.5$, $\frac{l}{S} = 5.0$, and $\alpha = 30^\circ$, which leads to a robot with the usable workspace defined by $R = 0.83S$ and $H = 1.10S$. According to these parameters relationships, a 3-PUU TPM can be designed to have a predefined size of the cylinder-usable workspace.

It is noticeable that the computational time of the optimization increases exponentially as the reducing of the interval sizes to get more accurate results, while optimization time may be reduced by other design approaches such as the interval analysis [27], genetic algorithm [29], etc.

V. DYNAMIC MODELING AND CONTROL ALGORITHM

A. Dynamic Modeling

The main issue in dynamic analysis for a parallel robot is to develop an inverse dynamic model, which enables the computation of the required actuator forces and/or torques when a desired trajectory of the moving platform is given. In what follows, we will perform the dynamic modeling of the 3-PUU TPM via the virtual work principle.

1) *Simplification Hypothesis*: As for a 3-PUU TPM, similar to a 3-PRS parallel manipulator [33], the complexity of the dynamic model partly comes from the three moving legs. Since the legs can be built with light materials such as aluminium alloy, the dynamic problem can be simplified by the following hypotheses: the rotational inertias of legs are neglected; the mass of each leg is equally divided into two portions and placed at its two extremities.

Let m_p , m_s , and m_l denote the mass of the moving platform, a nut and a leg, respectively. Then, the equivalent mass of the nut and the moving platform respectively becomes $\hat{m}_s = m_s + \frac{1}{2}m_l$ and $\hat{m}_p = m_p + \frac{3}{2}m_l$.

2) *Dynamic Modeling*: The torque $\boldsymbol{\tau} = [\tau_1 \ \tau_2 \ \tau_3]^T$ of the lead screw can be converted to the force $\mathbf{f} = [f_1 \ f_2 \ f_3]^T$ acting on the nut approximately by [34]

$$\mathbf{f} = 2\boldsymbol{\tau}/(\mu_c d_s) \quad (20)$$

where μ_c denotes the friction coefficient, and d_s represents the pitch diameter of the lead screw.

Let $\delta \mathbf{q} = [\delta d_1 \ \delta d_2 \ \delta d_3]^T$ and $\delta \mathbf{x} = [\delta p_x \ \delta p_y \ \delta p_z]^T$ be the vectors for virtual linear displacements of the nuts and moving platform, respectively. Applying the principle of virtual work allows the derivation of the following equation by neglecting the friction forces in passive U joints and assuming that there are no external forces suffered:

$$\mathbf{f}^T \delta \mathbf{q} + \mathbf{G}_s^T \delta \mathbf{q} - \mathbf{f}_s^T \delta \mathbf{q} + \mathbf{G}_p^T \delta \mathbf{x} - \mathbf{f}_p^T \delta \mathbf{x} = 0 \quad (21)$$

where $\mathbf{G}_s = \hat{m}_s g s \alpha \text{diag}\{1 \ 1 \ 1\}$ is the vector of gravity forces of the nuts with g representing the gravity acceleration, $\mathbf{G}_p = [0 \ 0 \ \hat{m}_p g]^T$ is the gravity force vector of the moving platform, $\mathbf{f}_s = \hat{m}_s [\ddot{d}_1 \ \ddot{d}_2 \ \ddot{d}_3]^T$ is the vector of inertial forces of the nuts, and $\mathbf{f}_p = \hat{m}_p [\ddot{p}_x \ \ddot{p}_y \ \ddot{p}_z]^T$ is the vector of inertial forces of the moving platform.

With the substitution of (5) into (21) and a careful treatment, one can obtain that

$$\mathbf{f} = \mathbf{M}_s \ddot{\mathbf{q}} + \mathbf{J}^{-T} \mathbf{M}_p \ddot{\mathbf{x}} - \mathbf{G}_s - \mathbf{J}^{-T} \mathbf{G}_p \quad (22)$$

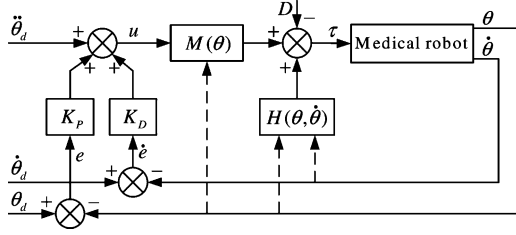


Fig. 6. Block diagram of joint space dynamic control for a 3-PUU TPM.

where $\mathbf{M}_s = \hat{m}_s \text{diag}\{1 \ 1 \ 1\}$ and $\mathbf{M}_p = \hat{m}_p \text{diag}\{1 \ 1 \ 1\}$.

Then, substituting (5) into (22) and in view of (2) and (20), results in the joint space dynamic model of a 3-PUU TPM:

$$\boldsymbol{\tau} = \mathbf{M}(\boldsymbol{\theta})\ddot{\boldsymbol{\theta}} + \mathbf{c}(\boldsymbol{\theta}, \dot{\boldsymbol{\theta}})\dot{\boldsymbol{\theta}} + \mathbf{G}(\boldsymbol{\theta}) \quad (23)$$

where

$$\mathbf{M}(\boldsymbol{\theta}) \equiv \frac{\mu_c d_s p}{4\pi} (\mathbf{M}_s + \mathbf{J}^{-T} \mathbf{M}_p \mathbf{J}^{-1}) \in \mathbb{R}^{3 \times 3} \quad (24)$$

$$\mathbf{c}(\boldsymbol{\theta}, \dot{\boldsymbol{\theta}}) \equiv \frac{\mu_c d_s p}{4\pi} (\mathbf{J}^{-T} \mathbf{M}_p \dot{\mathbf{J}}^{-1}) \in \mathbb{R}^{3 \times 3} \quad (25)$$

$$\mathbf{G}(\boldsymbol{\theta}) \equiv -\frac{\mu_c d_s}{2\pi} (\mathbf{G}_s + \mathbf{J}^{-T} \mathbf{G}_p) \in \mathbb{R}^3 \quad (26)$$

with $\boldsymbol{\theta} = [\theta_1 \ \theta_2 \ \theta_3]^T \in \mathbb{R}^3$ denoting the controlled variables, $\mathbf{M}(\boldsymbol{\theta})$ denoting a symmetric positive definite inertial matrix, $\mathbf{c}(\boldsymbol{\theta}, \dot{\boldsymbol{\theta}})$ representing the matrix of centrifugal and Coriolis forces, and $\mathbf{G}(\boldsymbol{\theta})$ describing the vector of gravity forces.

B. Dynamic Control Algorithm

The dynamic control in joint space utilizing the computed torque method is implemented for a 3-PUU TPM in this paper. Firstly, the joint space dynamic model (23) can be rewritten into the form

$$\mathbf{f} = \mathbf{M}(\boldsymbol{\theta})\ddot{\boldsymbol{\theta}} + \mathbf{H}(\boldsymbol{\theta}, \dot{\boldsymbol{\theta}}) \quad (27)$$

where $\mathbf{H}(\boldsymbol{\theta}, \dot{\boldsymbol{\theta}}) = \mathbf{c}(\boldsymbol{\theta}, \dot{\boldsymbol{\theta}})\dot{\boldsymbol{\theta}} + \mathbf{G}(\boldsymbol{\theta})$.

Fig. 6 represents a block diagram of the computed torque control system with proportional derivative (PD) feedback. Assuming that there are no external disturbances, then the manipulator is actuated with the following vector of joint forces:

$$\mathbf{f} = \hat{\mathbf{M}}(\boldsymbol{\theta})\mathbf{u} + \hat{\mathbf{H}}(\boldsymbol{\theta}, \dot{\boldsymbol{\theta}}) \quad (28)$$

where \mathbf{u} is an input signal vector in the form of acceleration, and $\hat{\mathbf{M}}(\boldsymbol{\theta})$ and $\hat{\mathbf{H}}(\boldsymbol{\theta}, \dot{\boldsymbol{\theta}})$ denote the estimators of the inertial matrix $\mathbf{M}(\boldsymbol{\theta})$ and the nonlinear coupling matrix $\mathbf{H}(\boldsymbol{\theta}, \dot{\boldsymbol{\theta}})$ implemented in the controller, respectively.

Combining (27) with (28) results in the following linear second-order system:

$$\ddot{\boldsymbol{\theta}} = \mathbf{u}. \quad (29)$$

The obtained linear system allows the specification of the necessary feedback gains as well as the reference signal required for a desired motion task, and the reference signal is defined according to the following algorithm [35]:

$$\mathbf{r} = \ddot{\boldsymbol{\theta}}_d + \mathbf{K}_D \dot{\boldsymbol{\theta}}_d + \mathbf{K}_P \boldsymbol{\theta}_d \quad (30)$$



Fig. 7. Photograph of a 3-PUU medical parallel robot prototype.

where $\boldsymbol{\theta}_d$ denotes the desired joint trajectory, and \mathbf{K}_P and \mathbf{K}_D represent the symmetric positive-definite feedback gain matrices.

The acceleration input signal in (29) then becomes

$$\begin{aligned} \mathbf{u} &= \mathbf{r} - \mathbf{K}_D \dot{\boldsymbol{\theta}} - \mathbf{K}_P \boldsymbol{\theta} \\ &= \ddot{\boldsymbol{\theta}}_d + \mathbf{K}_D (\dot{\boldsymbol{\theta}}_d - \dot{\boldsymbol{\theta}}) + \mathbf{K}_P (\boldsymbol{\theta}_d - \boldsymbol{\theta}). \end{aligned} \quad (31)$$

Substituting (31) into (29), leads to the equation of errors

$$\ddot{\mathbf{e}} + \mathbf{K}_D \dot{\mathbf{e}} + \mathbf{K}_P \mathbf{e} = 0 \quad (32)$$

where $\mathbf{e} = \boldsymbol{\theta}_d - \boldsymbol{\theta}$ is the vector of joint tracking errors, which will go to zero asymptotically by specifying appropriate values of feedback gains \mathbf{K}_P and \mathbf{K}_D .

VI. EXPERIMENTS ON THE PROTOTYPE

A prototype of a 3-PUU medical parallel robot is shown in Fig. 7, which was built in the Mechatronics Laboratory, University of Macau. The nominal kinematic and dynamic parameters of the robot prototype are described in Tables I and II, respectively, and the robot workspace is depicted in Fig. 4. It can be observed that the reachable workspace height is 152.1 mm and the usable workspace height can be calculated as 48.9 mm (with $R = 45.7$ mm), which is adequate for the CPR operation. It should be mentioned that this initial prototype is designed with respect to the performance of GDI and spatial utility ratio index according to [20], and the prototype is used here to validate the adopted model-based control algorithm with the dynamic modeling hypotheses.

TABLE II
DYNAMIC PARAMETERS OF THE 3-PUU TPM

Parameter	Value	Unit	Parameter	Value	Unit
m_p	0.4	kg	p	3.0	mm
m_s	0.4	kg	d_s	15.0	mm
m_l	0.2	kg	μ_c	0.1	—

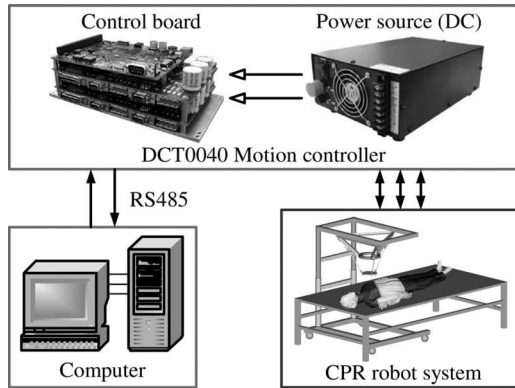


Fig. 8. Configuration of the experimental system setup.

Fig. 8 illustrates the hardware allocations and connections of the experimental system. The dynamic control algorithm has been implemented using a developed Visual C++ program running on a personal computer, and the three dc servomotors (from CM Technology, LLC) are controlled by a motion controller DCT0040 (from DynaCity Technology, Hong Kong, Ltd.), which is connected to the computer through a RS485 high-speed connection for the safety reason. The DCT0040 controller integrates motion control and servo amplifier into one unit to achieve space saving and to reduce wiring complexity, and is able to provide a good motion performance utilizing advanced digital signal processing (DSP) and field-programmable gate array (FPGA) technologies. The sampling frequency is 20 kHz.

The dynamic control is carried out such that the moving platform can track the following trajectory:

$$p_x = -30 \sin(\pi t) \quad (33a)$$

$$p_y = 30 \cos(\pi t) \quad (33b)$$

$$p_z = -110 + 20 \cos(\pi t/2) \quad (33c)$$

where t is the time variable in seconds, and p_x , p_y , and p_z are in millimeters. In the control procedure, the trajectory in task space is first translated into the joint space through inverse kinematic solutions, and the feedback gains are set as $\mathbf{K}_P = 625 \text{diag}\{1 \ 1 \ 1\}$ and $\mathbf{K}_D = 50 \text{diag}\{1 \ 1 \ 1\}$, respectively. The experimental results for the joint errors are plotted in Fig. 9. It can be observed that the tracking errors converge to almost steady zero errors only after about 0.3 s. The experimental results illustrate not only the applicability of the adopted control algorithm but also the rationality of the introduced simplifying hypothesis for the dynamic modeling process.

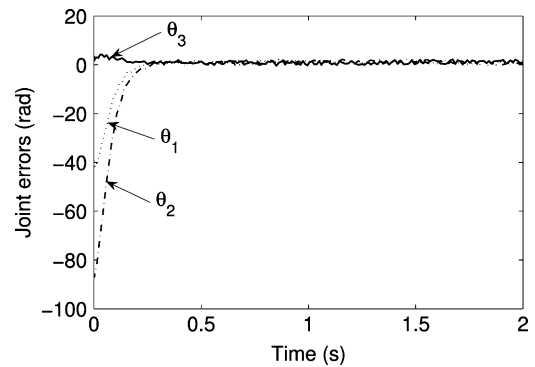


Fig. 9. Experimental results of dynamic control method.

VII. CONCLUSION

In this paper, a novel concept of employing a medical parallel robot for chest compressions in the process of CPR operation has been proposed. In view of the requirements from medical aspects, a 3-PUU translational parallel manipulator was chosen and designed to satisfy the specific requirement.

The kinematic analysis was performed and the manipulator-reachable workspace was generated by taking into account the physical constraints introduced by the rotational limits of universal joints and motion ranges of prismatic joints. Moreover, the usable workspace was also determined, which is defined as the maximum inscribed cylinder inside the reachable workspace, and all of the singular configurations are identified by means of the screw-theory approach. Furthermore, the optimal design is implemented based on a mixed index of the CI and GDI. The optimization leads to a robot possessing a large well-conditioning usable workspace excluding singularities. Then, by adopting a simplification hypothesis, the inverse dynamic model was established via the approach of virtual work principle, and the model-based control with PD feedback has been implemented. Experimental results illustrate both the validity of the adopted simplifying hypothesis and the good performance of the employed control algorithm.

The investigations presented here provide a sound base to develop a new medical robot to assist in CPR operation, which can significantly reduce the risk and workload of doctors in rescuing patients. Our further work will involve implementing animal experiments and clinical application for patients and establishing system models with the consideration of interactions between the moving platform and the human body to ensure that no harm will be happened to the ribs and heart of the patient. Furthermore, some monitoring sensors will also be used to detect whether the patient is awake or not so as to stop the CPR operation on time.

REFERENCES

- [1] I. N. Bankman, K. G. Gruben, H. R. Halperin, A. S. Popel, A. D. Guerci, and J. E. Tsitlik, "Identification of dynamic mechanical parameters of the human chest during manual cardiopulmonary resuscitation," *IEEE Trans. Biomed. Eng.*, vol. 37, no. 2, pp. 211–217, Feb. 1990.
- [2] T.-Q. Lou, X. Liu, X.-G. Bi, K.-X. Zhang, and Q.-F. Xie, "Analysis on diagnosis and treatment with integrated traditional Chinese and western medicine in 20 severe acute respiratory syndrome patients infected in

- hospital," *Chin. J. Integr. Traditional West. Med. Intensive Crit. Care*, vol. 10, no. 4, pp. 211–213, 2003.
- [3] L. W. Tsai, *Robot Analysis: The Mechanics of Serial and Parallel Manipulators*. New York: Wiley, 1999.
- [4] J.-P. Merlet, *Parallel Robots*. London, U.K.: Kluwer, 2000.
- [5] Y. Fang and L. W. Tsai, "Structure synthesis of a class of 4-DoF and 5-DoF parallel manipulators with identical limb structures," *Int. J. Robot. Res.*, vol. 21, no. 9, pp. 799–810, 2002.
- [6] X.-J. Liu and J. Wang, "Some new parallel mechanisms containing the planar four-bar parallelogram," *Int. J. Robot. Res.*, vol. 22, no. 9, pp. 717–732, 2003.
- [7] M. Carricato and V. Parenti-Castelli, "Kinematics of a family of translational parallel mechanisms with three 4-DOF legs and rotary actuators," *J. Robot. Syst.*, vol. 20, no. 7, pp. 373–389, 2003.
- [8] R. Di Gregorio, "A new family of spherical parallel manipulators," *Robotica*, vol. 20, no. 4, pp. 353–358, 2002.
- [9] X.-J. Liu, J. Wang, and G. Pritschow, "A new family of spatial 3-DoF fully-parallel manipulators with high rotational capability," *Mech. Mach. Theory*, vol. 40, no. 4, pp. 475–494, 2005.
- [10] M. Shoham, E. Zehavi, L. Joskowicz, E. Batkalin, and Y. Kunicher, "Bone-mounted miniature robot for surgical procedures: Concept and clinical applications," *IEEE Trans. Robot. Autom.*, vol. 19, no. 5, pp. 893–901, Oct. 2003.
- [11] H. Takanobu, T. Maruyama, A. Takanishi, K. Ohtsuki, and M. Ohnishi, "Mouth opening and closing training with 6-DOF parallel robot," in *Proc. IEEE Int. Conf. Robot. Autom.*, San Francisco, CA, 2000, pp. 1384–1389.
- [12] K. Homma, O. Fukuda, J. Sugawara, Y. Nagata, and M. Usuba, "A wire-driven leg rehabilitation system: Development of a 4-DOF experimental system," in *Proc. IEEE/ASME Int. Conf. Adv. Intell. Mechatron.*, Kobe, Japan, 2003, pp. 908–913.
- [13] R. Clavel, "Delta, a fast robot with parallel geometry," in *Proc. 18th Int. Symp. Ind. Robots*, Lausanne, Switzerland, 1988, pp. 91–100.
- [14] L. W. Tsai, G. C. Walsh, and R. E. Stamper, "Kinematics of a novel three DOF translational platform," in *Proc. IEEE Int. Conf. Robot. Autom.*, Minneapolis, MN, 1996, pp. 3446–3451.
- [15] D. Chablat, P. Wenger, F. Majou, and J.-P. Merlet, "An interval analysis based study for the design and the comparison of 3 DOF parallel kinematic machines," *Int. J. Robot. Res.*, vol. 23, no. 6, pp. 615–624, 2004.
- [16] L. W. Tsai and S. Joshi, "Kinematics analysis of 3-DOF position mechanisms for use in hybrid kinematic machines," *ASME J. Mech. Des.*, vol. 124, no. 2, pp. 245–253, 2002.
- [17] Y. Li and Q. Xu, "Kinematic analysis and design of a new 3-DOF translational parallel manipulator," *ASME J. Mech. Des.*, vol. 128, no. 4, pp. 729–737, 2006.
- [18] L. W. Tsai, "Kinematics of a three-DOF platform with three extensible limbs," in *Recent Advances in Robot Kinematics*, J. Lenarcic and V. Parenti-Castelli, Eds. Norwell, MA: Kluwer, 1996, pp. 401–410.
- [19] R. Di Gregorio and V. Parenti-Castelli, "A translational 3-DOF parallel manipulator," in *Advances in Robot Kinematics: Analysis and Control*, J. Lenarcic and M. L. Husty, Eds. Norwell, MA: Kluwer, 1998, pp. 49–58.
- [20] Y. Li and Q. Xu, "A new approach to the architecture optimization of a general 3-PUU translational parallel manipulator," *J. Intell. Robot. Syst.*, vol. 46, no. 1, pp. 59–72, 2006.
- [21] C. Gosselin and J. Angeles, "Singularity analysis of closed-loop kinematic chains," *IEEE Trans. Robot. Autom.*, vol. 6, no. 3, pp. 281–290, Jun. 1990.
- [22] C. Gosselin, "Determination of the workspace of 6-DOF parallel manipulators," *ASME J. Mech. Des.*, vol. 112, no. 3, pp. 331–336, 1990.
- [23] R. Di Gregorio and V. Parenti-Castelli, "Mobility analysis of the 3-UPU parallel mechanism assembled for a pure translational motion," *ASME J. Mech. Des.*, vol. 124, no. 2, pp. 259–264, 2002.
- [24] A. Wolf, M. Shoham, and F. C. Park, "Investigation of the singularities and self-motions of the 3-UPU robot," in *Advances in Robot Kinematics*, J. Lenarcic and F. Thomas, Eds. Norwell, MA: Kluwer, 2002, pp. 165–174.
- [25] D. Zlatanov, I. A. Bonev, and C. M. Gosselin, "Constraint singularities of parallel mechanisms," in *Proc. IEEE Int. Conf. Robot. Autom.*, Washington, DC, 2002, pp. 496–502.
- [26] S. A. Joshi and L. W. Tsai, "Jacobian analysis of limited-DOF parallel manipulators," *ASME J. Mech. Des.*, vol. 124, no. 2, pp. 254–258, 2002.
- [27] F. Hao and J.-P. Merlet, "Multi-criteria optimal design of parallel manipulators based on interval analysis," *Mech. Mach. Theory*, vol. 40, no. 2, pp. 157–171, 2005.
- [28] X.-J. Liu, "Optimal kinematic design of a three translational DoFs parallel manipulator," *Robotica*, vol. 24, no. 2, pp. 239–250, 2006.
- [29] D. Zhang, Z. Xu, C. M. Mechefske, and F. Xi, "Optimum design of parallel kinematic toolheads with genetic algorithms," *Robotica*, vol. 22, no. 1, pp. 77–84, 2004.
- [30] T. Yoshikawa, "Manipulability of robotic mechanisms," *Int. J. Robot. Res.*, vol. 4, no. 2, pp. 3–9, 1985.
- [31] C. Gosselin and J. Angeles, "A global performance index for the kinematic optimization of robotic manipulators," *ASME J. Mech. Des.*, vol. 113, no. 3, pp. 220–226, 1991.
- [32] O. Ma and J. Angeles, "Optimum architecture design of platform manipulators," in *Proc. IEEE Int. Conf. Adv. Robot.*, Pisa, Italy, 1991, pp. 1130–1135.
- [33] Y. Li and Q. Xu, "Kinematics and inverse dynamics analysis for a general 3-PRS spatial parallel mechanism," *Robotica*, vol. 23, no. 2, pp. 219–229, 2005.
- [34] R. J. Eggert, "Power screws," in *Standard Handbook of Machine Design*, J. E. Shisley and C. R. Mischke, Eds. New York: McGraw-Hill, 1996.
- [35] J. J. Craig, *Introduction to Robotics: Mechanics and Control*, 2nd ed. Reading, MA: Addison-Wesley, 1989.



Yangmin Li (M'98–SM'04) received the B.S. and M.S. degrees from Jilin University, Changchun, China, in 1985 and 1988, respectively, and the Ph.D. degree from Tianjin University, Tianjin, China, in 1994, all in mechanical engineering.

He was with South China University of Technology, the International Institute for Software Technology of the United Nations University (UNU/IIST), the University of Cincinnati, and Purdue University. He is currently an Associate Professor of robotics, mechatronics, control, and automation at the University of Macau, Macao SAR, China. He has authored or coauthored about 160 papers published in international journals and conference proceedings.

Dr. Li is a member of the American Society of Mechanical Engineers (ASME). Since 2004, he has been a Council Member and an Editor of the *Chinese Journal of Mechanical Engineering*.



Qingsong Xu received the B.S. degree in mechatronics engineering (with honors) from Beijing Institute of Technology, Beijing, China, in 2002, and the M.S. degree in electromechanical engineering from the University of Macau, Macao SAR, China, in 2004, where he is currently working toward the Ph.D. degree.

His current research interests include the design, kinematics, dynamics, and control of parallel robots, micromanipulators, flexible mechanisms, and mobile robots with various applications.